Trapped bubbles keep pumice afloat and gas diffusion makes pumice sink

Kristen E. Fauria[1], **Michael Manga**[1], **and Zihan Wei**[1, 2]

[1]*Department of Earth and Planetary Science, UC Berkeley, 307 McCone Hall, Berkeley, CA 94720-4767*

[2] *Department of Earth and Space Sciences, Peking University, Beijing, China*

Corresponding author: Kristen E. Fauria, kfauria@berkeley.edu

KEYWORDS

Buoyancy

Capillary processes

Percolation theory

Submarine volcanism

X-ray microtomography

ABSTRACT

Pumice can float on water for months to years – long enough for pumice to travel across oceans and facilitate the spread of species. Long-lived pumice floatation is unexpected, however, because pumice pores are highly connected and water wets volcanic glass. As a result, observations of long floating times have not been reconciled with predictions of rapid sinking. We propose a mechanism to resolve this paradox - the trapping of gas bubbles by water within the pumice. Gas trapping refers to the isolation of gas by water within pore throats such that the gas becomes disconnected from the atmosphere and unable to escape. We use X-ray microtomography to image partially saturated pumice and demonstrate that non-condensable gas trapping occurs in both ambient temperature and hot (500°C) pumice. Furthermore, we show that the size distribution of trapped gas clusters matches predictions of percolation theory. Finally, we propose that diffusion of trapped gas determines pumice floatation time. Experimental measurements of pumice floatation support a diffusion control on pumice buoyancy and we find that floatation time τ scales as $\tau \propto \frac{L^2}{D\theta^2}$ where L is the characteristic length of pumice, D is the gas-water diffusion coefficient, and θ is pumice water saturation. A mechanistic understanding of pumice floatation is a step towards understanding how pumice is partitioned into floating and sinking components and provides an upper bound on the lifetime of pumice rafts in the ocean.

1. INTRODUCTION

Pumice is a highly vesicular volcanic rock with a porosity high enough that it can float. Rafts of volcanic pumice can transit lakes and oceans and circle the globe (e.g., Richards, 1958; Risso et al., 2002; Bryan et al., 2004; von Lichtan et al., 2016). For example, pumice from the 1952 eruption of Volcán Barcena on Isla San Benedicto, 600 km west of Mexico, floated for at least 560 days and drifted over 8700 km (Richards, 1958). The 2012 eruption of Havre submarine volcano created a 1.5 km^3 pumice raft that spread over 550,000 km^2 within three months (Carey et al., 2014; Jutzeler et al., 2014). Pumice rafts have been shown to facilitate the dispersal of species such as barnacles, corals, algae, and gastropods (Bryan et al., 2012) because marine organisms grow on, and ocean currents advect, pumice (Richards, 1958; Jokiel, 1984; Bryan et al., 2004). While pumice rafts are relatively common and it is well known that ambient temperature pumice can float for long periods of time, the enduring buoyancy of pumice is surprising because pumice pores are almost entirely connected and water wets pumice (Whitham & Sparks, 1986; Vella & Huppert, 2007). Quantitative models for pumice saturation predict that ambient temperature pumice should sink orders of magnitude more rapidly than is observed (Vella & Huppert, 2007). The floatation time discrepancy between observations and the Vella & Huppert (2007) model suggests that simple gas displacement by an infiltrating water front is not sufficient to explain why ambient temperature pumice can float for years.

By comparison to ambient temperature pumice, hot pumice (e.g., >300°C) sinks almost immediately and the tendency for air-filled pumice to sink increases with pumice temperature (Whitham & Sparks, 1986; Dufek et al., 2007; Allen et al., 2008; Jutzeler et

al., 2016). Rapid water ingestion by hot pumice has been attributed to cooling-induced gas contraction (Whitham & Sparks, 1986; Cashman & Fiske, 1991; Allen et al., 2008) and hydrodynamic instabilities due to steam generation (Dufek et al., 2007). Air-filled hot pumice placed in water does not, however, completely saturate even at high (500°C) temperatures (Allen et al., 2008). As a result, we wish to understand how gas remains within initially hot pumice and what differences and similarities exist between saturation of ambient temperature and hot non-condensable gas filled pumice.

Pumice, with porosities of 50 to > 90 percent, is a porous medium. Water saturation of pumice is an example of two-phase flow in porous media and requires the replacement of a defending fluid (air or magmatic gases) with an invading fluid (liquid water). Two-phase flow in porous media has been widely studied in the context of the vadose zone, oil recovery, CO_2 sequestration, and gas sparging. In addition, water infiltration of pumice is a manifestation of a particular type of two-phase flow, imbibition, because water is the wetting phase. During imbibition the arrangement of fluid, or wetting pattern, can range from one where nearly all the pores are filled with the invading fluid to one where the defending fluid remains trapped in clusters (e.g., Lenormand & Zarcone, 1984). Trapped gas clusters (Figure 1), pockets of non-wetting fluid that are surrounded by the wetting fluid, are not only characteristic of two-phase flow in porous media but are very difficult to mobilize because of surface tension. Indeed, gas trapping is a mechanism employed for long term CO_2 sequestration (e.g., Ide et al., 2007; Benson & Cole, 2008).

We hypothesize that pumice floats for long periods of time because of the occurrence of gas trapping (either air or non-condensable magmatic gases) in isolated gas

clusters during water infiltration. We use X-ray microtomography to test the hypotheses that gas trapping occurs in both hot and ambient temperature pumice, that gas trapping can result in a high enough residual gas saturations to keep pumice afloat, and that percolation theory can describe gas trapping in pumice. While trapped gas may buoy pumice, we hypothesize that the outward diffusion of gas trapped in bubbles eventually causes pumice to sink. We test this gas diffusion hypothesis by conducting experiments where we measure the floatation time of dry and ambient temperature pumice on artificial seawater in a controlled laboratory setting. We then compare our results and pumice floatation times from four other studies with a prediction for pumice floatation time based on gas-diffusion out of a porous medium.

1.1 GAS TRAPPING IN POROUS MEDIA

Gas trapping has been observed in experiments, dictates wetting patterns, and controls residual non-wetting saturation of porous media (e.g., Blunt & Scher, 1995; Iglauer et al., 2013; Geistlinger & Mohammadian, 2015). A key element that promotes gas trapping is the slow advance of the invading fluid such that capillary forces dominate over viscous forces. In other words, the Capillary number

$$\mathrm{Ca} = \frac{v\mu}{\gamma}, \tag{1}$$

where v is the characteristic velocity, μ is the wetting fluid viscosity, and γ is surface tension on the interface between the two fluids, is very small, Ca << 1 (Lenormand & Zarcone, 1984; Wilkinson, 1984; Blunt & Scher, 1995).

We calculate a Capillary number for water infiltration into dry pumice using $\mu = 10^{-3}$ Pa s for the viscosity of water at room temperature, $\gamma = 0.072$ N m^{-1} for the surface tension at the air-water interface, and by estimating the velocity of water infiltrating

115 pumice using Darcy's law. For pumice floating on water, the maximum head gradient is
116 set by the hydrostatic pressure at the bottom edge of the pumice and the capillary
117 pressure. By assuming a constant pore radius and a hemispherical gas-water meniscus we
118 can write the liquid velocity as

119 $$v = \frac{\kappa}{\mu\phi}(\rho g h + \frac{2\gamma}{R}), \quad (2)$$

120 where κ is permeability, ϕ is connected porosity, ρ is water density, g is gravity, h is the
121 height of pumice in water, and R is pore throat radius. Pumice porosities can vary widely,
122 but typical values are 50 to 90 percent (pumice with rock equivalent densities between
123 2.4 and 3.0 g cm^{-3} must have porosities of at least 58 to 67 percent, respectively, to
124 initially float). Pumice permeabilities are more difficult to estimate, but measured values
125 range from 10^{-14} - 10^{-10} m^2 (e.g., Klug & Cashman, 1996; Tait et al., 1998; Saar &
126 Manga, 1999; Klug et al., 2002; Rust & Cashman, 2004, 2011; Muller et al., 2005;
127 Wright et al., 2006, 2009; Degruyter et al., 2010). We note that permeability may also be
128 a function of saturation, i.e., relative permeability is not unity. We consider pumice that is
129 immersed 0.01 – 1 m in water and pores that have radii of 0.1 – 0.001 mm. From these
130 input parameters, $3.8\text{x}10^{-11} < \text{Ca} < 4.3\text{x}10^{-4}$, which shows that capillary forces dominate
131 in pumice.

132 We also use pumice saturation measurements from Whitham & Sparks (1986) to
133 estimate water infiltration velocities according to,

134 $$v = \frac{\Delta V_w}{\Delta t S_a \phi} \quad (3)$$

135 where V_w is the volume of absorbed water, t is time, S_a is pumice surface area, and ϕ is
136 connected porosity. We estimate S_a by assuming the pumice clasts are spherical. Fourteen

pumice saturation measurements by Whitham and Sparks (1986) reveal average initial infiltration velocities over the first five minutes of water exposure of $2.74\pm0.97\times10^{-2}$ cm hr^{-1} and Capillary numbers of $7.62\pm2.69\times10^{-8}$. These Ca estimates indicate that capillary forces dominate. Thus, the saturation of pumice should be considered at the pore scale and may lead to gas trapping. In the next sections we introduce two mechanisms that allow gas trapping to occur, the percolation models that simulate them, and the gas-trapping predictions percolation theory makes.

1.1.1 Bypass trapping

Bypass trapping (Figure 1a) causes trapping through the sequential filling of pore throats such that the defending fluid becomes surrounded by the invading fluid before it can escape (e.g., Chatzis et al., 1983). Invasion percolation models simulate bypass trapping by (1) representing the porous medium as a network of spheres (pores) and cylinders (pore throats); (2) prescribing a capillary entry pressure for each throat and pore; and (3) filling throats and pores from highest to lowest pressure. As a result, a pore or series of pores with low capillary pressures may be completely surrounded before being filled and thus become trapped (but may contract or expand if compressible).

1.1.2 Snap-off trapping

Snap-off trapping occurs because for very low flow rates (or capillary numbers) the wetting fluid can flow along edges of the pore walls due to surface roughness (e.g., Leonard and Zarcone, 1984). This wall-hugging thin film can swell as the wetting fluid invades. As the film swells in the smallest throats, it completely displaces the non-wetting phase and can disconnect the non-wetting phase from any neighbors (Figure 1b). Snap-off trapping is simulated by Bond percolation. When snap-off and bypass trapping

160 are both possible, bypass trapping is favored because it occurs for higher capillary
161 pressures.

162 ***1.1.3 Percolation model predictions***

163 Both invasion and bond percolation theory make predictions about the size
164 distribution of residual trapped gas clusters. Because percolation systems are scale
165 invariant at the critical point (when fully percolated), the number of occurrences, *n(s*), of
166 trapped gas clusters containing *s* sites or pores scales according to a power-law,

167 $$n(s) \sim s^{-\beta}, \tag{4}$$

168 where $\beta = \frac{a+f}{f}$ and *a* is the spatial dimension and *f* is the fractal dimension of the
169 cluster. In 3D: $a = 3$, $f = 2.52$, and $\beta = 2.19$ (Stauffer, 1979; Wilkinson & Willemsen,
170 1983). The maximum size of the trapped gas cluster is limited by the samples size, *L*,
171 $s_{\max} \sim L^f$, (Wilkinson, 1986). Experimental studies of imbibition in porous media have
172 shown that trapped gas size distributions match Equation 4 (e.g., Geistlinger &
173 Mohammadian, 2015). Examining the size distribution of trapped gas bubbles in a natural
174 system, such as pumice, can therefore help distinguish if percolation theory (either Bond
175 or Invasion) applies.

176 **2. X-RAY MICROTOMOGRAPHY**

177 X-ray microtomography (μXRT) allows us to see both the internal structure of
178 pumice (e.g., Polacci et al., 2006; Wright et al., 2006; Degruyter et al., 2010; Giachetti et
179 al., 2011; Voltolini et al., 2011; Carey et al., 2013) and, when multiple fluids are present
180 within the pores, the distribution of those fluids (e.g., Wildenschild et al., 2002). We use
181 μXRT to (1) test the hypothesis that gas trapping occurs in pumice; (2) determine if

182 percolation theory can describe the size distribution of trapped gas; (3) examine the size
183 distribution of trapped gas for insights into the mechanisms (bypass or snap-off trapping)
184 that occur in pumice.

185 ***2.1 Experimental Set-Up***

186 We used μXRT to image the internal distribution of liquid and air in six uncut
187 pumice clasts. Before the μXRT, we conducted saturation experiments on ambient
188 temperature and hot (500°C) pumice from Santa Maria, Guatemala and Medicine Lake,
189 California (Table 1). We set ambient temperature pumice on a 13 wt% solution of
190 potassium iodide (KI) for ~20 hours such that the pumice could adsorb the liquid. KI, a
191 common chemical dopant, increases contrast of the μXRT images (greatly improves the
192 segmentation of air and water in the images), while maintaining a surface tension within
193 1% of water (Aveyard & Saleem, 1976; Wildenschild et al., 2002).

194 We heated two of the pumice samples (SM04 and SM05) to 500°C, quenched
195 these pumice clasts in the KI dopant, and allowed them to stay in the solution for ~10
196 minutes. All pumice pores were filled with air at the time of KI exposure. To preserve the
197 internal fluid distributions for μXRT imaging, we then rapidly removed and encased the
198 pumice in wax.

199 We carried out the μXRT imaging at the Lawrence Berkeley National Lab
200 Advanced Light Source on beamline 8.3.2. We conducted the scans using 30 kev
201 monochromatic X-Rays and a 5X lens (resolution of 1.22 μm/pixel). We used the
202 TomoPy gridrec algorithm to reconstruct the 3D image stacks (Gürsoy et al., 2014).

203 To minimize ring artifacts, we selected a subvolume from each data set of either
204 0.37 or 0.94 mm^3 for data processing. We used Fiji's Trainable Weka Segmentation

205 plugin - which employs multiple machine learning algorithms - to segment air, water, and
206 rock within each image sequence (Hall et al., 2009). To train classifiers for each image
207 sequence, we manually outlined vesicles and trapped air on fifty different images. After
208 checking and retraining the classifiers as necessary, we applied the trained classifiers
209 across the images sequences to segment air and rock (thereby creating two sets of
210 binarized image sequences for each sample).

211 We also made the image sequences binary by applying a greyscale threshold in
212 Fiji, but determined that the machine learning method reduced the effect of annular ring
213 artifacts and better preserved thin glass walls compared to the traditional threshold based
214 binarization method. Despite the advantages of the machine learning method, two image
215 sets (SM02 and SM05) had glass walls that were too thin to resolve and we do not report
216 porosities or vesicle size distributions for these samples.

217 After we segmented each data set, we loaded the binary images into Avizo where
218 we identified and quantified the volume, surface area, and orientation of individual
219 bubbles and vesicles. Here we refer to the pores of the pumice (that can be filled with
220 either gas or liquid) as vesicles and areas where the gas phase is present as bubbles.
221 Because most samples had highly interconnected porosities, we separated connected
222 vesicles using a watershed algorithm before measuring vesicles sizes and orientations
223 (supplementary information). No separation was applied to the gas bubbles. As a result,
224 any observed and reported gas bubbles were truly isolated. We note, however, that some
225 gas bubbles may appear connected (by one or two voxels) when they are not if glass
226 walls are thinner than one pixel. To correct for very thin glass walls we use a

227 "neighborhood" value of six in the Avizo labeling module such that bubbles must share at
228 least one voxel face to be considered connected.

229 Errors in generating the bubble and vesicle size distributions stem from two main
230 sources: (1) ring artifacts in the original greyscale image and (2) vesicle walls that are
231 thinner than the voxel resolution and that may also lead to overestimates of connected
232 porosity (Figure S1). Through examination of twenty 2D images from each dataset, we
233 estimate that ring artifacts result in the mischaracterization of gas or water in <1 volume
234 percent of each pumice. While the machine learning method for image segmentation
235 reduced the effects of ring artifacts compared to threshold based segmentation, it
236 introduced a number of very small (artifact) bubbles and vesicles that do not contribute to
237 the total volume fraction of pores or trapped gas. As a result, we filtered the data to
238 exclude any bubbles or vesicles with less than a 4 pixel radius or smaller than 10^{-6} mm^3.

239 ***2.3 X-ray microtomography results***

240 We find trapped gas clusters in all pumice we imaged (Figures 2 and 3). Trapped
241 gas cluster size varies and gas clusters fill part of, single, and multiple vesicles (Figures 2
242 and 3). Because connected porosities for most samples are close to or equal to the total
243 porosity, isolated gas pockets are due to trapping by liquid instead of isolation by rock
244 (Table 1). Furthermore, we found that ambient temperature pumice contain larger volume
245 percentages of trapped gas (36 - 50%) than the hot pumice (13 and 17%) (Table 1).

246 We use μXRT measurements of phase (liquid and water) saturations to estimate
247 pumice buoyancy, assuming glass densities of 2.4 g cm^{-3}, and find that the observed
248 trapped gas saturations are high enough to allow pumice to float. These density
249 calculations match our observation that many of the pumice clasts were floating or

neutrally buoyant when we encased them in wax. Our density calculation of ML01, however, does not match our observation that ML01 was not floating (Table 1). Discrepancies between observations and density estimages suggest that gas and liquid saturation within pumice is likely heterogeneous. Indeed, we visually observed areas of more and less gas saturation within μXRT images.

The size distributions of both trapped gas (black) and segmented pores (grey) are shown in Figure 4. For the majority of samples (ML02, SM01, SM02, and SM05) at least a third of the trapped gas is contained within one large cluster. These clusters, in cases where the vesicle size distributions are known (SM01 and ML02), greatly exceed the maximum vesicle size and Figure 3 shows how these largest trapped bubbles can extend throughout multiple vesicles. The trapped bubble size distributions, however, show that there are multiple modes of trapped bubbles sizes. In sample ML01, the trapped bubble size distribution mirrors the vesicle size distribution.

2.4 Comparison to Percolation Theories

Here we test the hypothesis that percolation theory can describe gas trapping in pumice by fitting Equation (4) to the observed distribution of trapped gas clusters using the maximum likelihood method (Clauset et al., 2009; Iglauer & Wülling, 2016). We find that Equation (4) fits the observed distributions well and that fitted power-law coefficients range from 1.51 - 2.10, which (other than the coefficient for ML01) are close to the value predicted by percolation theory ($\beta = 2.19$) (Figure 5; Table 1). These power-law fits lend support to a percolation theory treatment of pumice saturation.

Percolation theory also predicts:

$$A \propto V^{p},$$

where A is the surface area of the trapped clusters, and V is the volume of the trapped clusters (Stauffer, 1979). From our data sets, we empirically find $p = 0.75 – 0.83$ and the R^2 values for these fits are 0.95 - 0.99 (Table 1 and Figure S2). Values of p greater than 2/3 demonstrates that the gas bubbles are non-spherical.

3. MECHANISMS THAT CAUSE PUMICE TO SINK

The previous sections demonstrated that gas trapping occurs in pumice, that ambient temperature pumice traps more gas than hot (500°C) pumice, that gas trapping can lead to high enough residual gas saturations to allow pumice to float, and that percolation theory can describe the distribution of trapped gas clusters. The occurrence of gas trapping does not, however, explain why pumice, after floating for days or months, eventually sinks.

3.1 Pumice floatation experiments

To examine why pumice sinks, we conducted pumice floatation experiments using pumice from the 1902 plinian eruption of Santa Maria Volcano, Guatemala. We placed the pumice in artificial seawater and measured the time it took for the pumice to sink. Before the experiments, we cleaned the pumice in an ultrasonicator for four hours and dried the pumice in an oven at 65°C for 12 hours. We specifically chose a temperature lower than 100°C to ensure that we did not break pumice walls during the drying process and used μXRT to confirm that the pumice was dry prior to experiments. Table 2 shows the pumice weights, sizes, and characteristics. While we did not measure the volume of each pumice clast, we estimated volume by assuming porosities of 80% and glass densities of 2.4 g cm^{-3}.

To initiate the floatation experiments, we dropped the pumice from a height of 4 cm into individual containers of artificial seawater. These containers were covered to prevent evaporation and contamination. We monitored the pumice with a time lapse camera that could determine when each clast sank to the nearest minute.

3.2 Pumice floatation timescale

Here we propose that the diffusion of trapped gas bubbles out of the pumice (and eventually to the atmosphere) causes pumice containing trapped gas clusters to sink. We envisage that the diffusion process is analogous to Ostwald ripening where small (and thus higher pressure) trapped gas clusters diffuse into larger clusters and eventually to the atmosphere. If gas diffusion does control pumice buoyancy through time, then pumice floatation time should scale like a diffusive process where

$$\tau \sim \frac{L^2}{D_{eff}}, \tag{5}$$

and where L is the mean diameter of the pumice, and D_{eff} is the effective diffusion coefficient. The effective diffusion coefficient for trapped gas in pumice, as in other porous media, is not just the gas-liquid diffusion coefficient, but should be weighted by the connectivity of the porous media (i.e., porosity and partial saturation). From Hunt et al. (2014) we write effective diffusivity as $D_{eff} = D\theta^2$, where θ is water saturation (fraction of pore space filled by water) and D is the liquid-gas diffusion coefficient, such that

$$\tau \propto \frac{L^2}{D\theta^2}. \tag{6}$$

We test the hypothesis that diffusion of trapped gas out of pumice allows pumice to sink by comparing experimental measurements of pumice floatation time and volume

317 (Whitham and Sparks, 1986; Manville et al., 1998; Risso et al., 2002; White et al., 2001)
318 with Equation (6) and where $L \sim V^{2/3}$ (Figure 6). Because we do not know θ for any
319 individual pumice, and because, if our hypothesis is correct, θ changes through time, we
320 consider Equation (6) with a range of saturation values (8 - 80%).

321 **3.3 Pumice floatation results and model comparison**

322 Figure 6 shows measurements of floatation time and volume (this study and four others)
323 against predictions from Equation (6) and where $D = 1.9 \times 10^{-5}$ cm^2 s^{-1} is the air-water
324 diffusion coefficient at room temperature. Experimental measurements of pumice
325 floatation times generally match predictions from Equation (6) (Figure 6). We also list
326 pumice floatation times from our experiments in Table 2.

327 It is worth noting, however, that if pumice are highly non-spherical, then we
328 overestimate the effective length scale (shortest pumice axis). Furthermore, the timescale
329 for pumice floatation may depend strongly on θ, not only because θ affects the
330 diffusivity, but also because more diffusion must occur to sink a pumice with an initially
331 high trapped gas content.

332 While we are not the first to recognize that pumice floatation time scales like a
333 diffusive process (Manville et al., 1998), diffusion of trapped gas out of the pumice has
334 not previously been identified to be the controlling process. Figure 6, in combination with
335 observations of gas trapping, suggests that it is the diffusion of trapped gas out of pumice
336 that causes raft and other floating pumice to eventually sink.

337 **4. DISCUSSION**

338 **4.1 Gas trapping timescale**

We find that water saturation of pumice is a two-step process. First, capillary and hydrostatic pressures drive water into pores. Water invasion often leads to gas trapping (e.g. section 1.1) and ends when there are no longer pores to invade. Second, gas slowly diffuses out of trapped gas pockets thereby creating more space for the liquid (section 3). Here we estimate the timescale for the first of these processes - the time for pumice to reach its residual saturation state.

If pumice can be modeled as a bundle of horizontal parallel cylindrical tubes and capillary pressures drive fluid into the tubes, then the Washburn equation can describe the timescale for water saturation over horizontal distance L,

$$t = \frac{4L^2\mu}{\gamma d}, \quad (7)$$

where d is mean pore throat diameter. Equation (7) suggests that pumice with 0.05 mm diameter pores should reach its residual saturation state very rapidly: 2.7 seconds for 5 cm pumice and 18 minutes for 1 m pumice. In other words, if a dry pumice is set on water, then capillary forces draw in liquid quickly and set the wetting pattern and trapped gas geometry in timescale, t. We emphasize that pumice can remain buoyant following water invasion due to gas trapping.

4.2 Water saturation of hot versus cold pumice

We find that residual gas saturation is lower for hot pumice (500°C) compared to ambient temperature pumice, and that these lower gas saturations can account for the buoyancy differences of hot versus cold pumice (Table 1). Because hot pumice may rapidly saturate due to non-condensable gas contraction (Whitham & Sparks, 1986; Cashman &Fiske, 1991; Allen et al., 2008), we compare the pressure differences

generated by three processes that can drive fluid into pumice: water column weight, capillary action, and gas cooling and contraction.

Gravity induces a pressure difference when pumice is submerged in water proportional to,

$$\Delta P = (\rho_l - \rho_g) g L \sim 10^3 \text{ Pa}, \quad (8)$$

choosing L = 10 cm. The pressure difference induced by capillary forces is,

$$\Delta P = \frac{2\gamma}{R} \sim 1.5 \times 10^4 \text{ Pa}, \quad (9)$$

where R = 10 μm is pore throat radius. Lastly, the pressure difference created by gas contraction is proportional to the change in temperature of the gas by the ideal gas law such that

$$\Delta P = P_i \frac{\Delta T}{T_i} . \quad (10)$$

Assuming that the initial pressure, $P_{i,}$ of the gas is atmospheric (~10^5 Pa), the initial temperature of the gas, T_i, is 800 K, and the change in gas temperature, ΔT , is 500 K, then $\Delta P \sim 3.7 \times 10^4$ Pa.

Gas contraction can thereby produce pressure differences as large as those produced by capillary forces which suggests that, because pressure gradients drive fluid flow, gas contraction can be a relevant process for liquid ingestion. Furthermore, we expect that heat transfer from pumice to liquid is rapid (<1 s) because pumice walls are very thin,

$$t \sim L_w^2 / D_w, \quad (11)$$

where $L_w \sim 10^{-5}$ - 10^{-6} m is the glass wall thickness (Figure 2) and $D_w \sim 10^{-7}$ m^2 s^{-1} is water thermal diffusivity. Rapid heat transfer suggests that gas contraction occurs simultaneously with capillary induced pore filling. We note, however, that gas contraction may not proceed prior to pore filling because hot gas must contact cool liquid for heat transfer (e.g., Stroberg et al., 2010).

Following the derivation of the Washburn equation (Equation 7), we derive a new timescale for the initial stage of water ingestion into pumice when both gas contraction and capillary forces drive fluid flow:

$$t = \frac{4\mu L^2}{R^2\left(\frac{2\gamma}{R} + \frac{P_i \Delta T}{T_i}\right)} \quad . \tag{12}$$

Gas contraction in hot pumice may help to explain the differences in residual gas saturation of hot and cold pumice. When pressure doesn't change, according to the ideal gas law

$$\frac{V_i}{V_f} = \frac{T_i}{T_f} \quad , \tag{13}$$

where V_i and T_i are initial volume and temperature of gas within a pumice and V_f and T_f are final volume and temperature, respectively. We therefore expect that when air is cooled from 800 to 300 K, $V_f = 0.37 V_i$. Our experiments showed that hot pumice contained gas in ~23% of pore space while ambient temperature pumice retained gas in 54 - 79% of its pore space. This reduction in trapped gas volume is ~0.23/0.7 = 0.32 and is approximately the value (0.37) predicted by gas contraction alone.

Trapped bubble size distributions matched percolation theory for both hot and ambient temperature pumice (Figure 5). Invasion percolation theory works by prescribing

a capillary entry pressure for each pore and filling pores from highest to lowest entry pressure. Percolation theory may apply to hot and non-condensable gas-filled pumice because gas contraction introduces a new, yet additive, pressure difference across each pore and thus does not fundamentally change the mechanism for pore filling.

4.3 Bypass versus snap-off trapping

While the fit of Equation (4) to the measured trapped gas bubble size distributions supports a percolation theory control on pumice saturation, we have yet to determine if gas is trapped by bypass or snap-off mechanisms. The trapped bubble area-to-volume ratios show that the trapped bubbles are non-spherical (Table 1). Furthermore, we observe trapped gas within many interconnected pores (Figure 3). Because snap-off trapping leads to gas bubbles trapped in single pores (e.g., Figure 1), these observations support a bypass trapping mechanism. Furthermore, bypass trapping is topologically favored over snap-off trapping when both are possible.

4.4 Gas diffusion model

In section 3 we demonstrated that the slow diffusion of trapped gas bubbles causes pumice to eventually sink. Here we plot solutions to the diffusion equation to examine how pumice floatation time varies as a function of pumice size, porosity, and initial trapped gas saturation. To write a solution to the diffusion equation we make several assumptions: (1) pumice is spherical; (2) the binary water+gas mixture in pumice can be described as a continuum, (3) initial trapped gas saturation is uniform within the pumice, (4) the diffusion coefficient is constant, (5) pumice pores are entirely connected, and (6) the pumice is entirely submersed in water. With these assumptions in place, the average saturation ξ (gas volume/pore volume) in a spherical pumice of diameter L, with

initial interior gas saturation ξ_i, and with gas saturation equal to zero at the boundaries ± L/2 is

$$\xi(t) = \frac{6\xi_i}{\pi^2} \sum_{n=1}^{\infty} \frac{1}{n^2} e^{-D_{eff} n^2 \pi^2 t/(L/2)^2} \quad (14)$$

(Carslaw and Jaeger, 1959; Maneville et al., 1998). Here we let $D_{eff} = D\theta_i^2 = D(1-\xi_i)^2$ (e.g., Equation 6). Pumice sinks when its average density is equal to the density of the surrounding liquid such that

$$(1-\phi)\rho_r + \phi(1-\xi^*)\rho_l = \rho_l, \quad (15)$$

where ρ_r is the density of the solid phase, ξ^* is the gas saturation when a pumice is neutrally buoyant and ρ_l is the liquid density.

By combining Equations (14) and (15) we can calculate pumice floatation time, the time it takes a pumice to reach gas saturation ξ^*, as a function of pumice size L, porosity ϕ, and initial gas saturation ξ_i. Figure 7 shows solutions to Equations (14) and (15) using contours of constant floatation time. Figure 7 explores how pumice size, porosity, and initial gas saturation affect pumice floatation. We find that high porosity pumice need higher initial gas saturations to float for the same period of time as lower porosity pumice. Pumice size and porosity vary inversely along contours of constant floatation time and, for constant ϕ and ξ_i, larger pumice float longer.

5. CONCLUSIONS

In this paper, we explore the processes that allow pumice to float and sink. To do this, we studied pumice saturation at the scale of pore level processes where capillary forces may be relevant. From estimates of the capillary number - which indicate that surface tension dominates over viscous forces in pumice - we hypothesized that pumice

447 can trap isolated gas bubbles as water infiltrates its pores. We used X-ray
448 microtomography to determine if gas trapping occurs in pumice and found that both
449 ambient temperature and hot (500°C) pumice trap gas. We observed, however, that hot
450 pumice traps far less gas than ambient temperature pumice, consistent with the
451 observation that hot pumice (>300° C) often sinks after contact with water (Whitham &
452 Sparks, 1986; Allen et al., 2008; Jutzeler et al., 2016). That is, cold pumice can trap
453 enough gas to keep the pumice afloat while gas contraction in hot pumice leads to lower
454 residual gas saturations.

455 We examined the size distributions of trapped gas in both hot and ambient
456 temperature pumice and found that the distributions fit a power-law prediction from
457 percolation theory. The power-law fits support a percolation theory treatment of water
458 infiltration into pumice.

459 While trapped gas can buoy pumice, we hypothesized that outward diffusion of
460 the trapped gas clusters causes pumice to eventually sink. We quantified this hypothesis
461 with a model for pumice floatation time in terms of trapped gas diffusion (Equation 6).
462 To test the gas diffusion hypothesis, we conducted pumice floatation experiments and
463 compared Equation (6) to our results as well as data from four other studies. We found
464 that the observed pumice floatation times match a trapped gas diffusion prediction
465 (Figure 6). Furthermore, we plot solutions to the diffusion equation on a sphere to explore
466 pumice porosity, size, and initial gas saturation affect floatation time (Figure 7).

467 A mechanistic explanation for pumice floatation is an important step towards
468 understanding when and how pumice is partitioned into rafts versus submarine deposits
469 (e.g., Cashman & Fiske, 1991; Allen & McPhie, 2009; Rotella et al., 2013; Cas and

Giordano, 2014). Indeed, submarine volcanic deposits may not record eruption dynamics because non-condensable (i.e., CO_2 or air) gas trapping can make pumice buoyant. Furthermore, our results suggest that the lifetime of buoyant pumice rafts is not just limited by pumice abrasion (e.g., Carey et al., 2001; White et al., 2001), but also by gas diffusion. Non-condensable gas trapping and diffusion, by controlling pumice buoyancy, are therefore important controls on the transport and fate of pumice in the marine environment and location in the rock record.

ACKNOWLEDGMENTS

X-ray microtomography was enabled by access to the Lawrence Berkeley National Lab Advanced light source on beamline 8.3.2. We thank Dula Parkinson for guidance with μXRT imaging and image processing. A stimulating conversation with Alan Rempel helped to develop the initial gas trapping hypothesis. We thank Tushar Mittal for suggesting the machine learning segmentation algorithm and Steve Breen for informative discussions on percolation theory and for reviewing an earlier version of this manuscript. We thank Ray Cas, Thomas Giachetti, and *EPSL* editor Tamsin Mather for thoughtful reviews that contributed to this manuscript. Finally, we are grateful for support from Judy Webb and the US National Science Foundation. Data and code used in this study are available on VHub at https://vhub.org/resources/4117.

REFERENCES

Allen, S. R., Fiske, R. S., & Cashman, K. V. (2008). Quenching of steam-charged pumice: Implications for submarine pyroclastic volcanism. *Earth and Planetary Science Letters*, *274*(1-2), 40–49. http://doi.org/10.1016/j.epsl.2008.06.050

492 Allen, S. R., & McPhie, J. (2009). Products of neptunian eruptions. *Geology*, *37*(7), 639-
493 642.
494 Aveyard, R. & Saleem, S.M. (1975). Interfacial Tensions at Alkane-Aqueous
495 Electrolyte Interfaces, *Journal of the Chemical Society, Faraday Transactions 1:*
496 *Physical Chemistry in Condensed Phases*, *72*, 1609-1617..
497 Benson, S. M., & Cole, D. R. (2008). CO2 sequestration in deep sedimentary
498 formations. *Elements*, *4*(5), 325–331.
499 http://doi.org/10.2113/gselements.4.5.325
500 Blunt, M. J., & Scher, H. (1995). Pore-level modeling of wetting. *Physical Review E*,
501 *52*(6), 6387–6403. http://doi.org/10.1103/PhysRevE.52.6387
502 Bryan, S. E., Cook, a., Evans, J. P., Colls, P. W., Wells, M. G., Lawrence, M. G., … Leslie,
503 R. (2004). Pumice rafting and faunal dispersion during 2001-2002 in the
504 Southwest Pacific: Record of a dacitic submarine explosive eruption from
505 Tonga. *Earth and Planetary Science Letters*, *227*(1-2), 135–154.
506 http://doi.org/10.1016/j.epsl.2004.08.009
507 Bryan, S. E., Cook, A. G., Evans, J. P., Hebden, K., Hurrey, L., Colls, P., … Firn, J. (2012).
508 Rapid, long-distance dispersal by pumice rafting. *PLoS ONE*, *7*(7).
509 http://doi.org/10.1371/journal.pone.0040583
510 Carey, S., Morelli, D., Sigurdsson, H., & Bronto, S. (2001). Tsunami deposits from major
511 explosive eruptions: an example from the 1883 eruption of Krakatau. *Geology*,
512 *29*(4), 347-350. doi: 10.1130/0091-7613(2001)
513

514 Carey, R. J., Manga, M., Degruyter, W., Gonnermann, H., Swanson, D., Houghton, B., ...
515 & Patrick, M. (2013). Convection in a volcanic conduit recorded by bubbles.
516 *Geology*, *41*(4), 395-398.
517 Carey, R. ., Wysoczanski, R., Wunderman, R., & Jutzeler, M. (2014). Discovery of the
518 Largest Historic Silicic Submarine Eruption. *Eos, Transactions American*
519 *Geophysical Union*, *95*(19), 2012–2014.
520 Cas, R. A., & Giordano, G. (2014). Submarine volcanism: a review of the constraints,
521 processes and products, and relevance to the Cabo de Gata volcanic succession.
522 *Italian Journal of Geosciences*, *133*(3), 362-377.
523 Cashman, K. V., & Fiske, R. S. (1991). Fallout of pyroclastic debris from submarine
524 volcanic eruptions. *Science(Washington)*, *253*(5017), 275-280.
525 Chatzis, I., Morrow, N., & Lim, H. (1983). Magnitude and detailed structure of
526 residual oil saturation. *Old SPE Journal*, *23*(2), 311–326.
527 http://doi.org/10.2118/10681-PA
528 Carslaw, H. S., & Jaeger, J. C. (1959). Conduction of heat in solids. *Oxford: Clarendon*
529 *Press, 1959, 2nd ed.*
530 Clauset, A., Shalizi, C. R., & Newman, M. E. (2009). Power-law distributions in
531 empirical data. *SIAM review*, *51*(4), 661-703.
532 http://dx.doi.org/10.1137/070710111
533 Degruyter, W., Bachmann, O., & Burgisser, A. (2010). Controls on magma
534 permeability in the volcanic conduit during the climactic phase of the Kos
535 Plateau Tuff eruption (Aegean Arc). *Bulletin of Volcanology*, *72*(1), 63–74.
536 http://doi.org/10.1007/s00445-009-0302-x

537 Dufek, J., Manga, M., & Staedter, M. (2007). Littoral blasts: Pumice-water heat transfer
538 and the conditions for steam explosions when pyroclastic flows enter the ocean.
539 *Journal of Geophysical Research: Solid Earth*, *112*(B11).
540 Geistlinger, H., & Mohammadian, S. (2015). Capillary trapping mechanism in
541 strongly water wet systems: Comparison between experiment and percolation
542 theory. *Advances in Water Resources*, *79*, 35–50.
543 http://doi.org/10.1016/j.advwatres.2015.02.010
544 Giachetti, T., Burgisser, A., Arbaret, L., Druitt, T. H., & Kelfoun, K. (2011). Quantitative
545 textural analysis of Vulcanian pyroclasts (Montserrat) using multi-scale X-ray
546 computed microtomography: comparison with results from 2D image analysis.
547 *Bulletin of volcanology*, *73*(9), 1295-1309.
548 Gürsoy, D., De Carlo, F., Xiao, X., & Jacobsen, C. (2014). TomoPy: a framework for the
549 analysis of synchrotron tomographic data. *Journal of synchrotron radiation*, *21*(5),
550 1188-1193.
551 http://doi.org/10.1107/S1600577514013939
552 Hall, M., Frank, E., Holmes, G., Pfahringer, B., Reutemann, P., & Witten, I. H. (2009).
553 The WEKA data mining software: an update. *ACM SIGKDD explorations*
554 *newsletter*, *11*(1), 10-18.
555 http://doi.org/10.1145/1656274.1656278
556 Hunt, A., Ewing, R., & Ghanbarian, B. (2014). *Percolation theory for flow in porous*
557 *media* (Vol. 880). Springer.
558 Ide T., S., Jessen, K., & Orr, F. M. (2007). Storage of CO2 in saline aquifers: Effects of
559 gravity, viscous, and capillary forces on amount and timing of trapping.

560 *International Journal of Greenhouse Gas Control*, *1*(4), 481–491.
561 http://doi.org/10.1016/S1750-5836(07)00091-6
562 Iglauer, S., Paluszny, A., & Blunt, M. J. (2013). Simultaneous oil recovery and residual
563 gas storage: A pore-level analysis using in situ X-ray micro-tomography. *Fuel*,
564 *103*, 905–914. http://doi.org/10.1016/j.fuel.2012.06.094
565 Iglauer, S., & Wülling, W. (2016). The scaling exponent of residual non-wetting phase
566 cluster size distributions in porous media. *Geophysical Research Letters*.
567 http://doi.org/ 10.1002/2016GL071298
568 Jokiel, P. L. (1984). Long distance dispersal of reef corals by rafting. *Coral Reefs*, *3*(2),
569 113–116. http://doi.org/10.1007/BF00263761
570 Jutzeler, M., Marsh, R., Carey, R. J., White, J. D. L., Talling, P. J., & Karlstrom, L. (2014).
571 On the fate of pumice rafts formed during the 2012 Havre submarine eruption.
572 *Nature Communications*, *5*, 3660. http://doi.org/10.1038/ncomms4660.
573 Jutzeler, M., M. Manga, J.D.L. White, P.J. Talling, A.A. Proussevitch, S.F.L. Watt, M.
574 Cassidy, R.N. Taylor, A. Le Friant, and O. Ishizuka, Submarine deposits from
575 pumice-rich pyroclastic density currents dispersing over water: an
576 outstanding example from offshore Montserrat (IODP 340), *Bulletin of the*
577 *Geological Society of America*, in press.
578 Klug, C., & Cashman, K. V. (1996). Permeability development in vesiculating
579 magmas: implications for fragmentation. *Bulletin of Volcanology*, *58*(2-3), 87–
580 100. http://doi.org/10.1007/s004450050128
581 Klug, C., Cashman, K., & Bacon, C. (2002). Structure and physical characteristics of
582 pumice from the climactic eruption of Mount Mazama (Crater Lake), Oregon.
583 *Bulletin of Volcanology*, *64*(7), 486–501. http://doi.org/10.1007/s00445-002-

584 0230-5
585 Lenormand, R., & Zarcone, C. (1984). Role of roughness and edges during imbibition in
586 square capillaries. In *SPE annual technical conference and exhibition*. Society of
587 Petroleum Engineers.
588 Manville, V., White, J. D. L., Houghton, B. F., & Wilson, C. J. N. (1998). The saturation
589 behaviour of pumice and some sedimentological implications. *Sedimentary*
590 *Geology*, *119*(1-2), 5–16. http://doi.org/10.1016/S0037-0738(98)00057-8
591 Polacci, M., Baker, D. R., Mancini, L., Tromba, G., & Zanini, F. (2006). Three-
592 dimensional investigation of volcanic textures by X-ray microtomography and
593 implications for conduit processes. *Geophysical Research Letters*, *33*(13).
594 Richards, A. F. (1958). Transpacific distribution of floating pumice from Isla San
595 Benedicto, Mexico. *Deep Sea Research (1953)*, *5*(1), 29–35.
596 http://doi.org/http://dx.doi.org/10.1016/S0146-6291(58)80005-3
597 Risso, C., Scasso, R. A., & Aparicio, A. (2002). Presence of large pumice blocks on
598 Tierra del Fuego and South Shetland islands shorelines, from 1962 South
599 Sandwich Islands eruption. *Marine Geology*, *186*(3-4), 413–422.
600 http://doi.org/10.1016/S0025-3227(02)00190-1
601 Rust, A. C., & Cashman, K. V. (2004). Permeability of vesicular silicic magma: Inertial
602 and hysteresis effects. *Earth and Planetary Science Letters*, *228*(1-2), 93–107.
603 http://doi.org/10.1016/j.epsl.2004.09.025
604 Rust, A. C., & Cashman, K. V. (2011). Permeability controls on expansion and size
605 distributions of pyroclasts. *Journal of Geophysical Research: Solid Earth*,
606 *116*(11), 1–17. http://doi.org/10.1029/2011JB008494

607 Saar, M. O., & Manga, M. (1999). Permeability-porosity relationships in vesicular
608 basalts. *Geophysical Research Letters*, *26*(1), 111–114.
609 Stauffer, D. (1979). Scaling Theory of Percolation Clustgers. *Physics Reports-Review*
610 *Section of Physics Letters*, *54*(1), 1–74.
611 Stroberg, T. W., Manga, M., & Dufek, J. (2010). Heat transfer coefficients of natural
612 volcanic clasts. *Journal of Volcanology and Geothermal Research*, *194*(4), 214-219.
613 Tait, S., Thomas, R., Gardner, J., & Jaupart, C. (1998). Constraints on cooling rates and
614 permeabilities of pumice in an explosive eruption jet from colour and magnetic
615 mineralogy. *Journal of Volcanology and Geothermal Research*, *86*(1-4), 79–91.
616 http://doi.org/10.1016/S0377-0273(98)00075-4
617 Vella, D., & Huppert, H. E. (2007). The waterlogging of floating objects. *Journal of*
618 *Fluid Mechanics*, *585*, 245. http://doi.org/10.1017/S002211200700715X
619 Voltolini, M., Zandomeneghi, D., Mancini, L., & Polacci, M. (2011). Texture analysis of
620 volcanic rock samples: quantitative study of crystals and vesicles shape preferred
621 orientation from X-ray microtomography data. *Journal of Volcanology and*
622 *Geothermal Research*, *202*(1), 83-95.
623 von Lichtan, I. J., White, J. D. L., Manville, V., & Ohneiser, C. (2016). Giant rafted
624 pumice blocks from the most recent eruption of Taupo volcano, New Zealand:
625 Insights from palaeomagnetic and textural data. *Journal of Volcanology and*
626 *Geothermal Research*, *318*, 73-88.
627 White, J. D. L., Manville, V., Wilson, C. J. N., Houghton, B. F., Riggs, N. R., & Ort, M.
628 (2001). Settling and deposition of AD 181 Taupo pumice in lacustrine and
629 associated environments, in White, J.D.L, and Riggs, N.R., eds., *Volcaniclastic*

630 *Sedimentation in Lacustrine Settings:* Oxford, UK, Blackwell Science, p. 141-150,
631 doi:10.1002/9781444304251.ch7
632 Whitham, A.G., & Sparks, R. S. J. (1986). Pumice, *Bulletin of Volcanology*, *48*(4), 209-
633 223.
634 Wildenschild, D., Vaz, C. M. P., Rivers, M. L., Rikard, D., & Christensen, B. S. B. (2002).
635 Using X-ray computed tomography in hydrology: Systems, resolutions, and
636 limitations. *Journal of Hydrology*, *267*(3-4), 285–297.
637 http://doi.org/10.1016/S0022-1694(02)00157-9
638 Wilkinson, D., & Willemsen, J. F. (1983). Invasion percolation: a new form of
639 percolation theory. *Journal of Physics A: Mathematical and General*, *16*(14),
640 3365–3376. http://doi.org/10.1088/0305-4470/16/14/028
641 Wilkinson, D. (1984). Percolation model of immiscible displacement in the presence of
642 buoyancy forces. *Physical Review A*, *30*(1), 520.
643 Wilkinson, D. (1986). Percolation effects in immiscible displacement. *Physical Review A*,
644 *34*(2), 1380.
645 Wright, H. M. N., Roberts, J. J., & Cashman, K. V. (2006). Permeability of anisotropic
646 tube pumice: Model calculations and measurements. *Geophysical Research*
647 *Letters*, *33*(17), 2–7. http://doi.org/10.1029/2006GL027224
648 Wright, H. M. N., Cashman, K. V., Gottesfeld, E. H., & Roberts, J. J. (2009). Pore
649 structure of volcanic clasts: Measurements of permeability and electrical
650 conductivity. *Earth and Planetary Science Letters*, *280*(1-4), 93–104.
651 http://doi.org/10.1016/j.epsl.2009.01.023
652 **FIGURES**

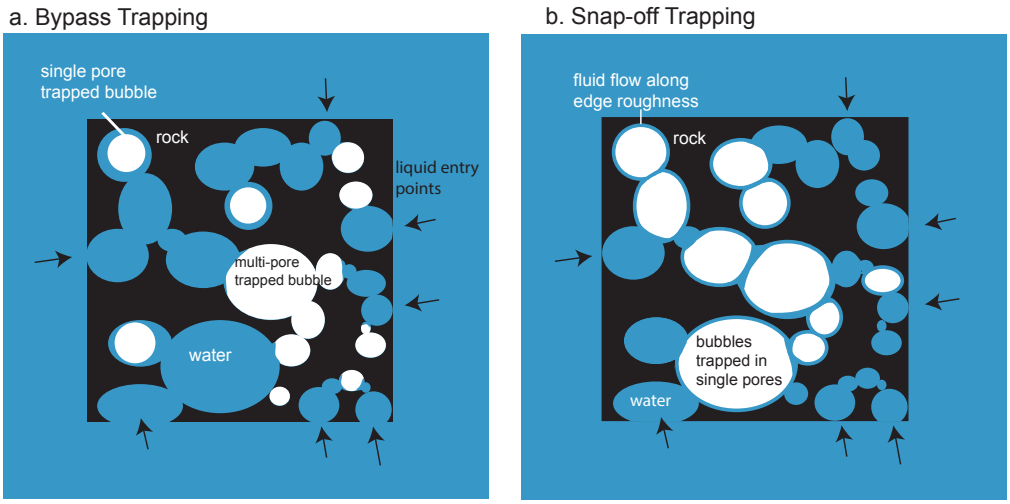

653
654 **Figure 1:** Mechanisms of gas trapping. Illustrations of gas trapping by (a) bypass and (b)
655 snap-off trapping in pumice with connected pores. In both cases capillary forces draw
656 water into pores such that water completely surrounds the gas phase and the gas is unable
657 to escape.
658

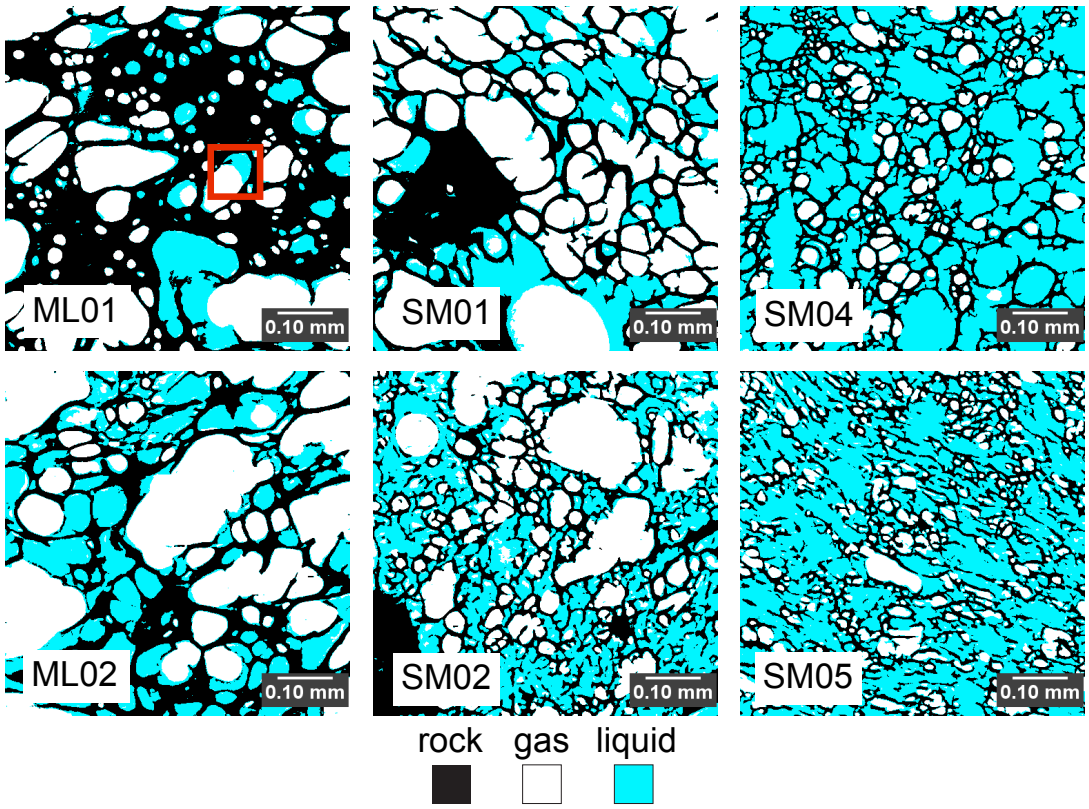

659

660 **Figure 2:** X-ray microtomography images. 2D μXRT images of pumice containing water
661 and trapped gas. While hot pumice (SM04 and SM05) contain trapped gas, they hold
662 smaller volume percentages compared to ambient temperature pumice. Contacts between
663 rock, liquid, and gas demonstrate that the liquid is the wetting fluid (see red box). While
664 glass walls are too thin to resolve in places (particularly in SM02 and SM05), we do not
665 see any evidence in the μXRT that the thin glass walls in pumice are broken or damaged
666 due to cleaning in an ultrasonic bath.

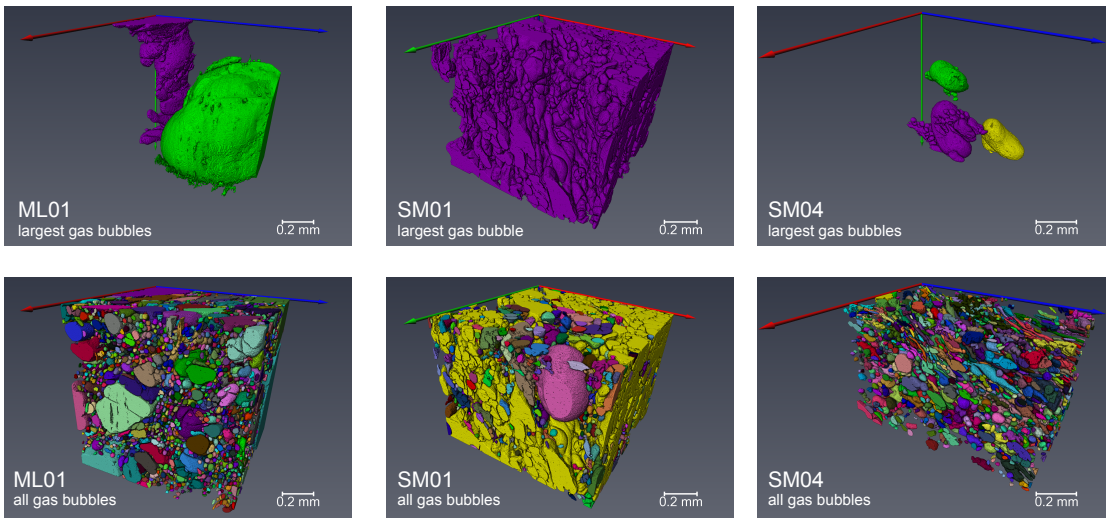

667
668 **Figure 3:** Shapes of trapped gas bubbles. 3D μXRT images of trapped gas bubbles within
669 pumice. Colors in this figure are chosen at random to identify separate gas bubbles. The
670 top rows show the largest gas bubbles and the bottom row shows all gas bubbles within a
671 single pumice. A single interconnected gas bubbles extends throughout many pores in
672 pumice SM01.
673

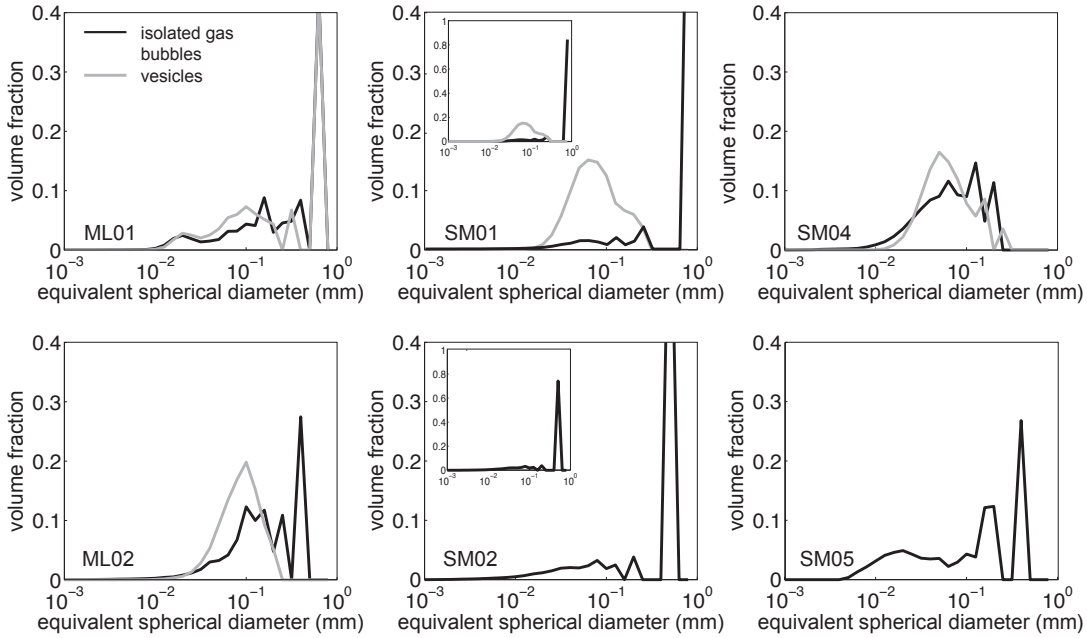

674

675 **Figure 4:** Bubble and vesicle size distributions. Trapped gas bubbles, locations where
676 only the gas is present, are shown in black, and vesicles, pumice pores that can be filled
677 with liquid or gas, are in grey. At least a third of the trapped gas is contained with a
678 single large bubble for most of samples. The existence of large trapped bubbles, in
679 combination with the vesicle size distribution, demonstrates that at least the largest gas
680 clusters often extend through multiple pores. Bubbles and vesicles are binned into fifty
681 logarithmically spaced bins and each bin is divided by the total volume of air or vesicles.
682 Volume fraction is not weighted by bin width such that the sum of all bins equals one.

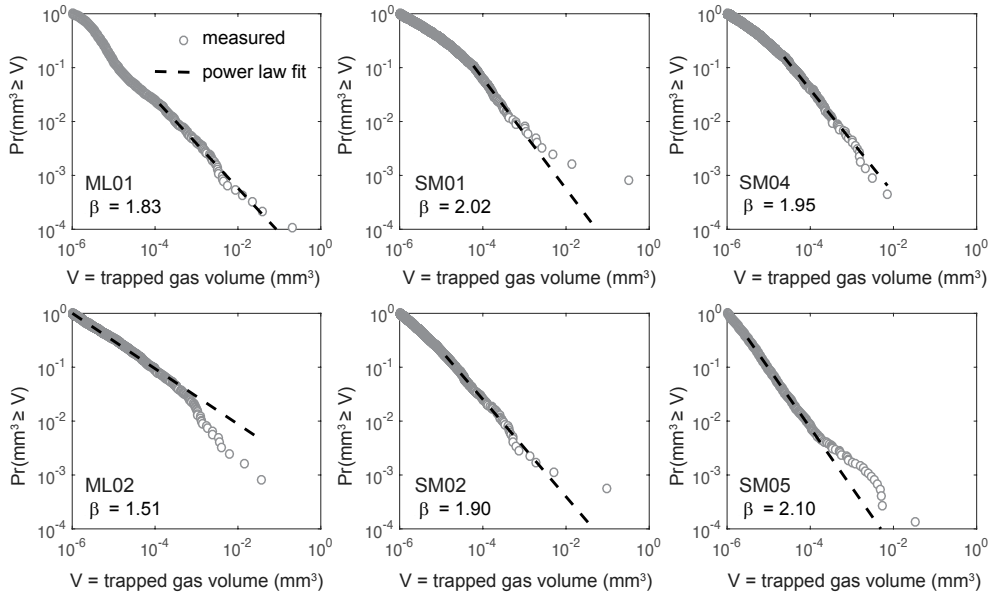

683
684 **Figure 5:** Power-law fits of bubble-size distributions. Measured distributions of trapped
685 bubble volume (grey circles) and the fitted power-law distributions (dashed lines). The y-
686 axis shows the probability that a bubble is larger than a given volume, V. With the
687 exception of ML02, the fitted power-law coefficients, β, are consistent with the value
688 predicted from percolation theory, $\beta = 2.19$. Because our machine learning segmentation
689 method generated very small (artifact) bubbles, we removed bubbles smaller than 10^{-6}
690 mm^3 before fitting a power-law coefficient.
691
692
693

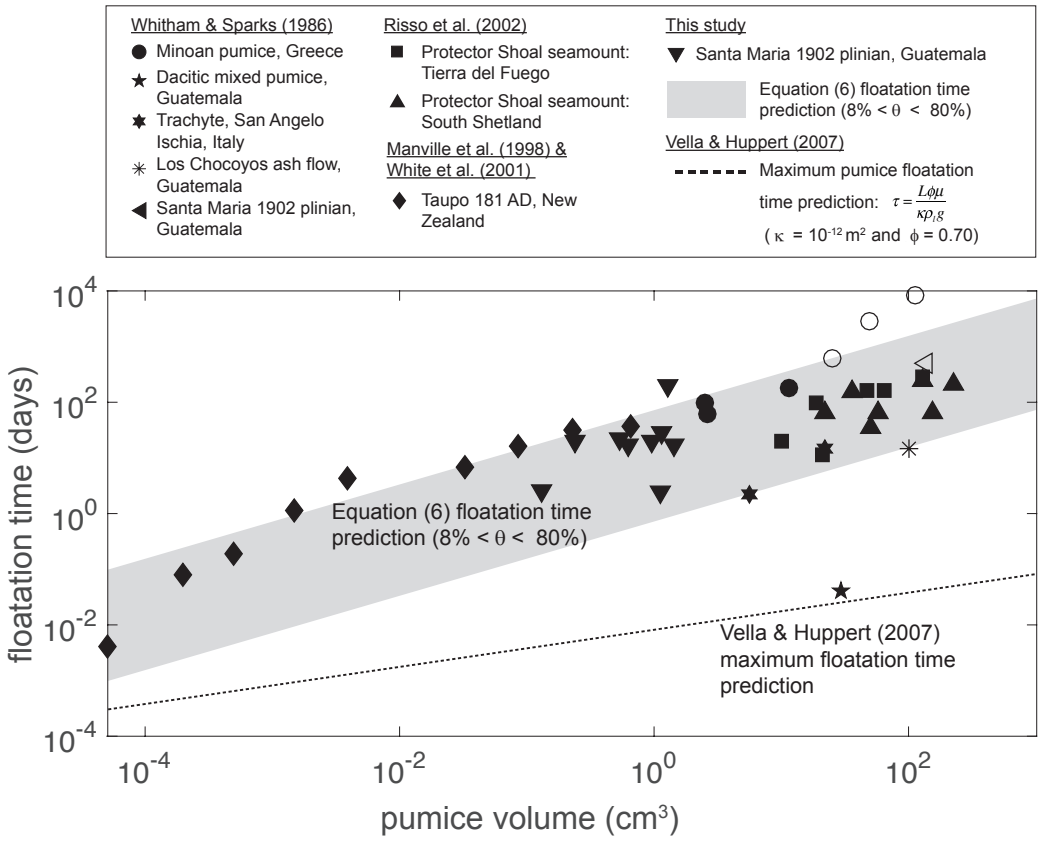

694
695
696 **Figure 6:** Floatation time as a function of pumice volume. Measurements of pumice
697 floatation from this study, Whitham & Sparks (1986), Maneville et al. (1998), Risso et al.
698 (2002), and White et al. (2001). Pumice floatation time predictions from this study
699 (Equation 6) and Vella & Huppert (2007) are also shown. Measured floatation times fit
700 the trend predicted by Equation (6) (grey bar). Filled symbols represent measured
701 sinking times while open symbols represent projected sinking times.

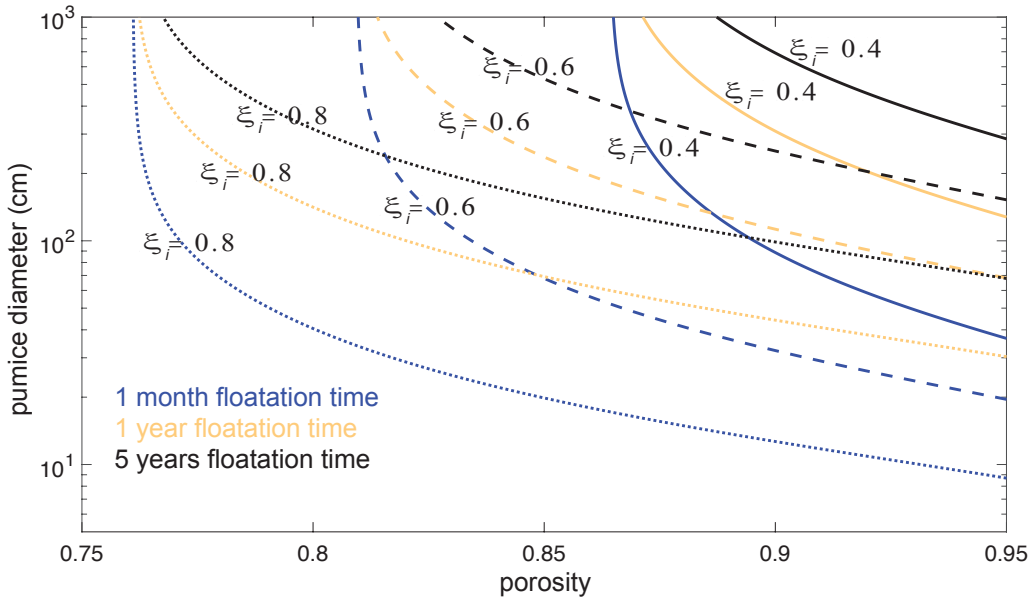

Figure 7: Floatation time as a function of clast size, porosity and initial saturation. We plot solutions to Equations (14) and (15) to demonstrate how floatation time varies with pumice size, porosity, and initial gas saturation, ξ_i. We assume ρ_r = 2.4 g cm^{-3}, ρ_r = 1.0 g cm^{-3}, and sum the first ten terms of Equation (14).

TABLES

Table 1: μXRT samples (uncut clasts) and measurements

sample name	SM01	SM02	SM04	SM05	ML01	ML02
sample description	1902 Santa Maria	1902 Santa Maria	1902 Santa Maria	1902 Santa Maria	Medicine Lake	Medicine lake
pumice mass (g)	0.07	0.19	0.13	0.04	0.15	0.76
pumice dimensions mm^3	9 x 4.5 x 4	11 x 7 x4.5	11 x 6 x 5	6.5 x 3 x 3	9.5 x 5 x 5	5 x 5 x 4
temperature	ambient	ambient	500 ˚C	500 ˚C	ambient	ambient
ending buoyancy	floating	neutrally buoyant	not floating	not floating	not floating	barely floating
porosity	0.70	NA	0.73	NA	0.63	0.67
connected porosity	0.70	NA	0.73	NA	0.55	0.65
liquid volume/ total volume	0.30	NA	0.56	NA	0.13	0.31
gas volume/total volume	0.40	0.36	0.17	0.13	0.50	0.36
liquid saturation (liquid volume/pore volume)	0.43	NA	0.77	NA	0.21	0.46
calculated wet density/ KI density	0.86	NA	1.07	NA	0.83	0.93
trapped gas bubble number density (cm^{-3})	$9.6x10^5$	$3.0x10^6$	$4.4x10^6$	$4.2x10^6$	$7.2x10^6$	$2.3x10^6$
vesicle number density (cm^{-3})	$8.3x10^6$	NA	$1.5x10^7$	NA	$9.6x10^6$	$5.3x10^6$
β: Power law exponent	2.02	1.90	1.95	2.10	1.83	1.51
smallest bubble fit to power law (mm^3)	$5.9x10^{-5}$	$1.3x10^{-5}$	$2.3x10^{-5}$	$3.1x10^{-6}$	$1.3x10^{-4}$	$1.0x10^{-6}$
p: Trapped bubble volume to surface area exponent	0.82	0.82	0.77	0.76	0.75	0.83
size of analyzed volume (mm^3)	0.94	0.37	0.37	0.94	0.94	0.37

While μXRT analysis is done on subvolumes of larger clasts, we expect the subvolumes to be representative of the larger pumice in part because the pumice are relatively small

(i.e., < 1 g). Furthermore, the selected pumice samples do not have bread crust textures such that we expect differences between rim an internal porosities to be minimal.

Table 2: Floatation time measurements for Santa Maria pumice.

sample name	dry weight (g)	estimated volume (cm^3)	floatation time (days)
SM_F02	0.30	0.63	17.3
SM_F03	0.25	0.53	22.7
SM_F05	0.46	0.95	20.2
SM_F06	0.68	1.42	17.0
SM_F09	0.61	1.28	195.5
SM_F10	0.06	0.13	2.6
SM_F11	0.55	1.15	28.2
SM_F21	0.54	1.12	2.5
SM_F22	0.12	0.24	20.1

Notation

v	velocity
μ	dynamic viscosity
γ	surface tension
ρ	density
g	gravity
κ	permeability
ϕ	connected porosity
h	height
V_w	volume of water absorbed
t	time
S_a	pumice surface area
n	number of occurences
s	sites or pores
β	power law coefficient
a	spatial dimension
f	fractal dimension a cluster
s_{max}	maximum size of a trapped gas cluster
L	pumice diameter
A	surface area of trapped gas clusters
V	trapped gas volume
p	power-law coefficient
τ	pumice floatation timescale
D_{eff}	effective diffusion coefficient

θ	water saturation
D	liquid-gas diffusion coefficient
d	mean pore throat diameter
P	pressure
R	pore throat radius
T	temperature
L_w	glass wall thickness
D_w	water thermal diffusivity
T_i	initial temperature
T_f	final temperature
V_i	initial volume
V_f	final volume
ξ	gas saturation
ξ_i	initial gas saturation
ξ^*	neutral buoyancy gas saturation
ρ_r	glass density
ρ_l	liquid density